Real-time detection of voltage patterns in the brain

Tomas Fiers

Thesis submitted for the degree of
Master of Science in
Biomedical Engineering

Thesis supervisors:
Prof. dr. ir. A. Bertrand
Prof. dr. F. Kloosterman

Assessors:
Prof. dr. ir. R. Puers
Dr. eng. J. Couto

Mentors:
Ir. J. Wouters
Dott. D. Ciliberti

Academic year 2018 – 2019

Abstract − 30 Nov

Contents

Abbreviations

BPF Band-pass filter. See chapter 2.

CA1 Cornu ammonis, region 1. Region in the hippocampus where voltages are recorded from (see **????**).

CA3 Cornu ammonis, region 3. Region in the hippocampus (see **????**). CA3 sends many axons (called "Schafer collaterals") to CA1.

GEVec Generalized eigenvector. See section 3.4.

GEVal Generalized eigenvalue. See section 3.4.

LFP Local field potential. The extracellular electric potential (see **??**).

RMS Root-mean-square.

RNN Recurrent neural network. See chapter 4.

SWR Sharp wave-ripple. The pattern in the LFP that we want to detect in real-time. See **??**.

SNR Signal-to-noise ratio. See section 3.2.

SOTA State of the art. The algorithm currently used for SWR detection, namely an online single channel band-pass filter.

Symbols

Notation

y Scalars are denoted in lowercase italic.

$\mathbf{z}$ Vectors are denoted in lowercase boldface.

$\mathbf{A}$ Matrices are denoted in uppercase boldface.

$\odot$ Elementwise multiplication. ("Hadamard product").

$\sigma(\cdot)$ Sigmoid 'squashing' function. $\sigma(x) = \frac{1}{1+\exp(-x)}, \quad \in (0,1)$.

$\tanh(\cdot)$ Hyperbolic tangent. $\tanh(x) = 2 \ \sigma(x) - 1, \quad \in (-1,1)$.

Signals

$\mathbf{z}_t$ Digitized LFP sample at discrete time step t. $\mathbf{z}_t \in \mathbb{R}^C$, with C the number of channels (i.e. the number of electrodes simultaneously recorded from). Input to an SWR detection algorithm.

o_t Output signal of an SWR detection algorithm, $\in \mathbb{R}$.

n_t 'Envelope'. Transformation of o_t, so that it is constrained to $\mathbb{R}^+$. Should be high when the corresponding input sample $\mathbf{z}_t$ is part of an SWR segment, and low when it is not. $n_t = |o_t|$ for online linear filters; $n_t = \sigma(o_t)$ for the RNN's of chapter 4.

y_t Binary target signal, used when training data-driven SWR detection algorithms. We define $y_t = 1$ when the corresponding input sample $\mathbf{z}_t$ is part of an SWR segment, and $y_t = 0$ when it is not.

Measures & parameters

P Precision. Also known as positive predictive value. The fraction of correct detections versus all detections.

R Recall. Also known as sensitivity, hit rate, or true positive rate. The fraction of detected reference SWR segments versus all reference SWR segments.

F_β F-score: weighted harmonic mean of recall and precision. $F_\beta = \frac{(1+\beta^2)PR}{\beta^2 P + R}$. Measures detection performance "for a user who attaches β times as much importance to recall as to precision." [1]

F_1 F-score where recall and precision are weighted equally. For the common case where the PR-curve is concave, $F_1(T)$ is maximal when $P(T) = R(T) (= F_1(T))$.

T Detection threshold applied to the envelope n_t, $T \in (\min n_t, \ \max n_t)$. Each threshold T yields a different P-value, R-value, F_1-value, etc.

Glossary

Apical   The 'top' side of a pyramidal neuron. In the neocortex: the side near the skull. In CA1: the 'stratum radiatum' side (see **??**).

Basal   The 'bottom' side of a pyramidal neuron. In the neocortex: the side towards the center of the brain. In CA1: the 'stratum oriens' side (see **??**).

Tetrode   Four thin electrode wires ($< 30\,\mu m$ in diameter), bundled together.

Neurite   Either an axon or a dendrite.

Schafer collateral   Axon originating in CA3 and terminating in CA1.

Soma   (plural: somata). Cell body of a neuron.

Introduction − 9 Nov [9p]

1.1   Closed-loop brain-computer interfaces [1p]

1.2   Sharp wave-ripples [6p]

Description [2p]

Scientific importance [2p]

Biophysics [1p]

Closed-loop technology [1p]

1.3   Problem statement [1p]

1.4   Thesis overview [1p]

Single-channel linear filtering − 26 Oct [10p]

2.1   **Offline labelling of SWR segments [3p]**

2.2   **State of the art online SWR detectors [3p]**

2.3   **Quantifying & comparing detectors [4p]**

Multi-channel linear filtering − 19 Oct [10p]

3.1 Data-driven algorithms [1p]

In this and the following chapter, we describe *supervised*, or *data-driven* detection algorithms: they require training data $\mathbf{z}_t^{\text{train}}$, and an associated labelling y_t^{train} which marks when there is an event present in $\mathbf{z}_t^{\text{train}}$. We arbitrarily define $y_t \in \{0, 1\}$, with $y_t = 1$ when the corresponding input sample $\mathbf{z}_t$ is part of an SWR segment, and $y_t = 0$ when it is not.

The problem of obtaining a reference target labelling y_t for some recording data $\mathbf{z}_t$ is the same as marking SWR segments for offline analysis or for offline evaluation of an online detection algorithm. As described in section 2.1, this can be done either by human expert labellers, or by using an automated *offline* SWR detection algorithm, where we assume that the automated labelling corresponds well to a supposed human expert labelling. In this thesis, we use the automated labelling method of section 2.1 to generate target labellings y_t^{train}.

Before a supervised algorithm can be used for real-time detection, its parameters have to be 'tuned'. This is done using a training dataset $(\mathbf{z}_t^{\text{train}}, y_t^{\text{train}})$, during the so called *training phase*. Parameters are changed such that the algorithm's output o_t for an input $\mathbf{z}_t^{\text{train}}$ matches the target labelling y_t^{train} well. Sections 3.2 and 4.2 describe how this tuning can be done for two concrete detection algorithms.

The hope is that the trained algorithm also performs well on input data $\mathbf{z}_t^{\text{test}}$ not part of the training set. That is, that the algorithm has good *generalization performance*. When this is not the case and the algorithm is tuned so that it only performs well on the training data, we say that the algorithm has been *overfit*. Often, so called *regularization* methods exist to discourage overfitting on the training data. Some example regularization methods are discussed in sections 3.7 and 4.3.
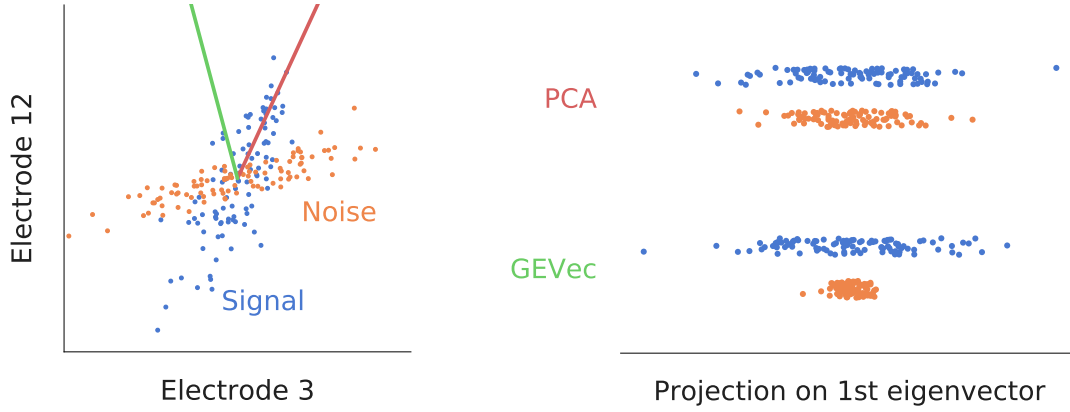
Figure 3.1: **Linear signal-to-noise maximisation**. Toy example to illustrate the generalized eigenvector approach to signal detection. *Left*: multi-channel time-series data plotted in 'phase space' (meaning without time axis), with blue dots representing samples where the signal was present, and orange dots representing samples where it was not. Actually toy data drawn from two 2-dimensional Gaussian distributions with different covariance matrices. Red vector: first eigenvector of the signal covariance matrix (also known as the first principal component). Green vector: first generalized eigenvector of the signal and noise covariance matrices. *Right*: Projection of both data sets on both the ordinary eigenvector ("PCA") and the generalized eigenvector ("GEVec"). The ratio of the projected signal data variance versus the projected noise data variance is maximised for the GEVec case.

3.2   Linear signal-to-noise maximisation [2p]

In this chapter, we search for a linear combination of channels that yields an output signal o_t useful for sharp wave-ripple detection. More precisely, we search for a vector $\mathbf{w} \in \mathbb{R}^c$ in channel (or electrode) space to project the samples $\mathbf{z}_t \in \mathbb{R}^c$ on, so that the output signal

$$o_t = \mathbf{w}^T \mathbf{z}_t \tag{3.1}$$

has high variance (or power) during SWR events, and low variance outside them.[1] This principle is illustrated with a two-dimensional toy dataset in fig. 3.1. We can then detect SWR events using threshold crossings of the envelope of o_t, as discussed in section 2.2.

The next two sections describe how this vector $\mathbf{w}$ can be found.

3.3   The optimisation problem

Suppose all training samples $\mathbf{z}_t^{\text{train}}$ are gathered and divided over two data matrices $\mathbf{S} \in \mathbb{R}^{C \times N_S}$ and $\mathbf{N} \in \mathbb{R}^{C \times N_N}$, where $\mathbf{S}$ (for 'signal') contains all N_S samples of $\mathbf{z}_t^{\text{train}}$

---

[1]We assume that the input signals are zero-mean, such that the power P of the output signal equals its variance: $P_o = \langle o_t^2 \rangle = \langle (o_t - \mu_o)^2 \rangle = \text{Var}(o_t)$ when $\mu_o = 0$, which is the case for zero-mean input channels: $\mu_o = \langle o_t \rangle = \langle \mathbf{w}^T \mathbf{z}_t \rangle = \sum_i w_i \langle z_{t,i} \rangle = 0$ when $\langle z_{t,i} \rangle = 0$ for all channels i.
This zero-mean assumption is reasonably well fulfilled for the analysed recording: the sample values of a 10-second moving average of the recording have a median of -0.02 µV and an interquartile range of 0.13 µV. In comparison, the RMS-value of the recording is 210 µV.

where an SWR is present, and $\mathbf{N}$ (for 'noise') contains all N_N other samples. (These matrices can be easily constructed by concatenating all segments in $\mathbf{z}_t^{\text{train}}$ where an SWR is present, and all segments where there is no SWR present).

Equation (3.1) then becomes, in vector notation:

$$\mathbf{o}_S = \mathbf{w}^T \mathbf{S}$$
$$\mathbf{o}_N = \mathbf{w}^T \mathbf{N},$$

where each element of the row vectors $\mathbf{o}_S$ and $\mathbf{o}_N$ corresponds to one (multichannel) sample of $\mathbf{S}$ or $\mathbf{N}$. Figure 3.1 (right) shows the distribution of the values in two example data vectors $\mathbf{o}_S$ and $\mathbf{o}_N$.

We want to find the weight vector $\widehat{\mathbf{w}}$ that maximises the variance of $\mathbf{o}_S$ versus the variance of $\mathbf{o}_N$, i.e.

$$\widehat{\mathbf{w}} = \arg\max_{\mathbf{w}} \frac{\text{Var}(\mathbf{o}_S)}{\text{Var}(\mathbf{o}_N)} \tag{3.2}$$

$$= \arg\max_{\mathbf{w}} \frac{\frac{1}{N_S}\mathbf{o}_S\mathbf{o}_S^T}{\frac{1}{N_N}\mathbf{o}_N\mathbf{o}_N^T}$$

$$= \arg\max_{\mathbf{w}} \frac{\frac{1}{N_S}\mathbf{w}^T\mathbf{S}\mathbf{S}^T\mathbf{w}}{\frac{1}{N_N}\mathbf{w}^T\mathbf{N}\mathbf{N}^T\mathbf{w}}$$

In this last equation, we recognize the empirical covariance matrices $\mathbf{R}_{SS}$ and $\mathbf{R}_{NN}$, which are defined as:

$$\mathbf{R}_{SS} = \frac{1}{N_S}\mathbf{S}\mathbf{S}^T \tag{3.3}$$

$$\mathbf{R}_{NN} = \frac{1}{N_N}\mathbf{N}\mathbf{N}^T \tag{3.4}$$

$\mathbf{R}_{SS} \in \mathbb{R}^{C \times C}$ and $\mathbf{R}_{NN} \in \mathbb{R}^{C \times C}$ are symmetric matrices, where each diagonal element yields the variance of a channel, and each off-diagonal element yields the covariance between a pair of channels.

The condition for the optimal weight vector, eq. (3.2), is thus equivalent to:

$$\widehat{\mathbf{w}} = \arg\max_{\mathbf{w}} \frac{\mathbf{w}^T\mathbf{R}_{SS}\mathbf{w}}{\mathbf{w}^T\mathbf{R}_{NN}\mathbf{w}} \tag{3.5}$$

In appendix B, we show that the solution $\widehat{\mathbf{w}}$ to this optimisation problem is the first so called "generalized eigenvector" of $(\mathbf{R}_{SS}, \mathbf{R}_{NN})$.

3.4 The generalized eigenproblem

An arbitrarily scaled vector $\mathbf{w}_i$ is a so called *generalized eigenvector* (GEVec) for the ordered matrix pair $(\mathbf{R}_{SS}, \mathbf{R}_{NN})$ when the following holds:

$$\mathbf{R}_{SS}\mathbf{w}_i = \lambda_i\mathbf{R}_{NN}\mathbf{w}_i, \tag{3.6}$$

for some scalar λ_i, which is called the *generalized eigenvalue* (GEVal) corresponding to $\mathbf{w}_i$. The largest scalar λ_1 for which eq. (3.6) holds is the 'first' GEVal, and as mentioned before, the corresponding GEVec $\mathbf{w}_1$ is the solution $\widehat{\mathbf{w}}$ to eq. (3.5).

Since the 1960's, numerically stable algorithms exist that solve the generalised eigen-problem eq. (3.6) [2]. A specialized algorithm is applicable when the input matrices are symmetric – as is the case for $\mathbf{R}_{SS}$ and $\mathbf{R}_{NN}$. This algorithm (based on a Cholesky factorization and the classical QR-algorithm for ordinary eigenproblems) is implemented in the LAPACK software package (as `ssygv` and `dsygv`), and can be easily accessed using e.g. the `eig` function from MATLAB, or the `eigh` function from SciPy's `linalg` module.

3.5   Result for SWR detection

We divided the 34-minute long LFP recording into two datasets. The first 60% was used as training data, to calculate the covariance matrices $\mathbf{R}_{SS}$ and $\mathbf{R}_{NN}$, and to calculate from these the optimal linear combination of channels $\widehat{\mathbf{w}}$, as described in the preceding sections. The remaining 40% was used to evaluate this filter $\widehat{\mathbf{w}}$, and to compare it to the state-of-the-art method (the single-channel online band-pass filter).

Figure 3.2A shows an excerpt of the test input signal, and the corresponding filter output envelopes (blue for state-of-the art method, orange for GEVec-based multichannel method. Filter outputs o_t are rectified to obtain envelopes $n_t = |o_t|$). Additional excerpts are shown in fig. C.1. The elements of $\widehat{\mathbf{w}}$ (i.e. the filter weights) are visualized in fig. 3.2B.

It is clear that the GEVec filter output indeed has high power during SWR events, as promised by theory. The filter weights and input-output excerpts reveal that the GEVec output is composed mainly of a few channels in the stratum radiatum (channels 4-5-6 here), where they pick up the sharp waves. However, the filter output envelope is also high for sharp wave-like activity on the stratum radiatum channels without or with only very weak ripple activity in the higher channels: see figs. C.1a, C.1b and C.1d. This results in false positive detections.

We also notice some premature detections (figs. C.1a and C.1c), where the sharp wave – and thus also the GEVec filter output – of an SWR-complex already has high power before the ripple has started. The GEVec detection then happens before the start of the reference SWR-segment, which is based on ripple power. These early detections thus count (arguably unfairly so) as false positives, under the evaluation scheme that we use.

This effect, where the sharp wave is discernible before the ripple, results in faster detections when the detection *does* fall within the reference segment. When all 468 SWR events from the training set are analysed, we find a large improvement in detection latency: at thresholds where both methods detect 80% of these reference SWR segments, the median absolute detection latency drops from 24 ms for the state-of-the-art online band-pass filter to 12 ms for the GEVec-based filter. The relative detection latency drops by 32.5 percentage points, from 58.1% to 25.6%. Similar latency improvements are found for other recall and precision values: see fig. 3.3.

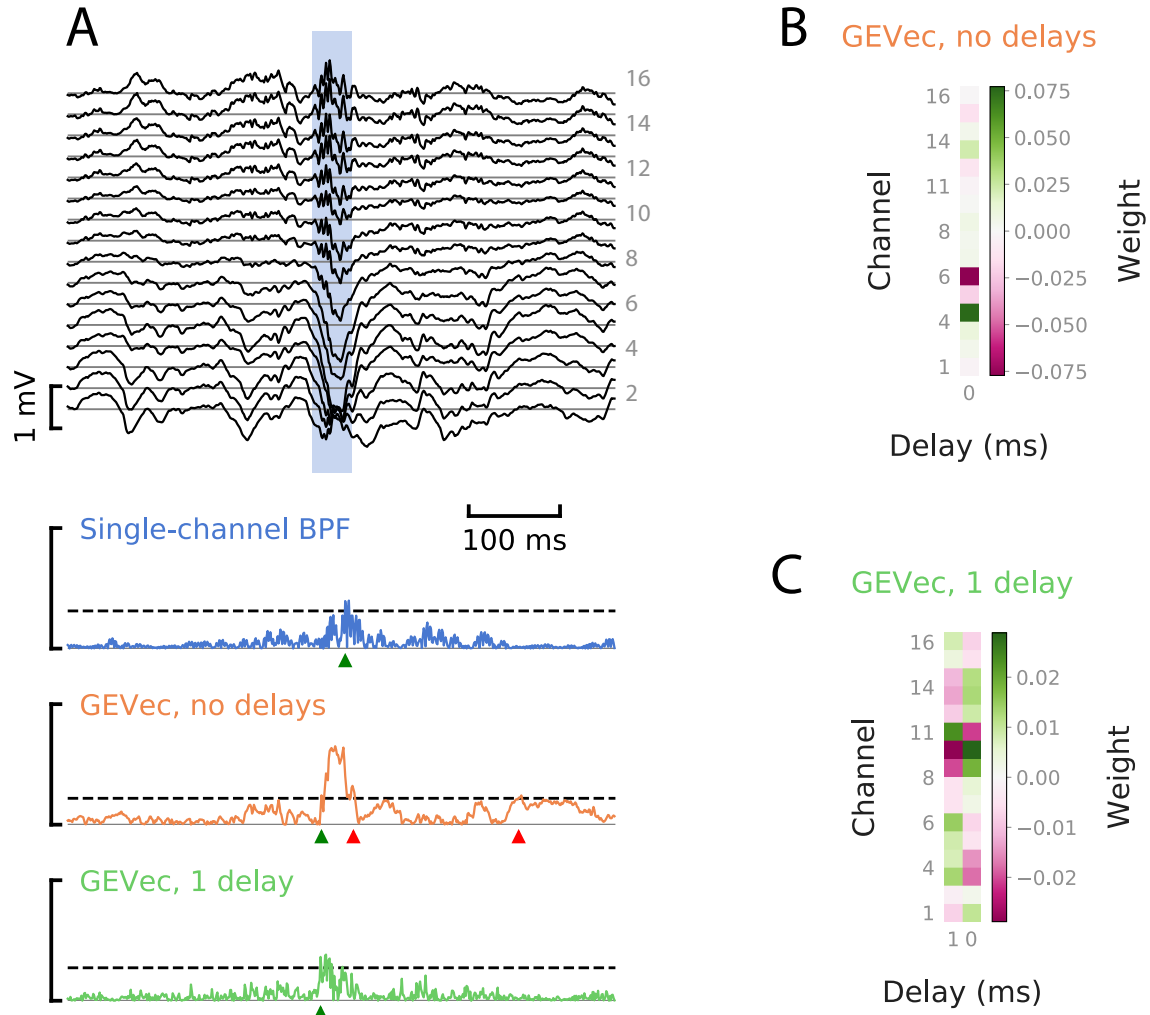This strong improvement in detection latency trades off with an increase in false positives,

Figure 3.2: **Linear, SNR-maximising combinations of electrodes**.
A. Example input and output signals. *Top*: multi-channel LFP, $\mathbf{z}_t$. Light-blue vertical band: a reference SWR segment. *Bottom*: output envelopes $\mathbf{n}_t$, for different filtering algorithms. Dashed horizontal lines: detection thresholds, chosen so that each algorithm reaches a recall value of 80%. Green triangles: correct detections. Red triangles: incorrect detections.
B. Generalised eigenvector $\widehat{\mathbf{w}}$ (i.e. the weights of the multichannel filter), for a purely spatial filter.
C. Generalised eigenvector $\widehat{\mathbf{w}}$ for a spatiotemporal filter with a one-sample delay.
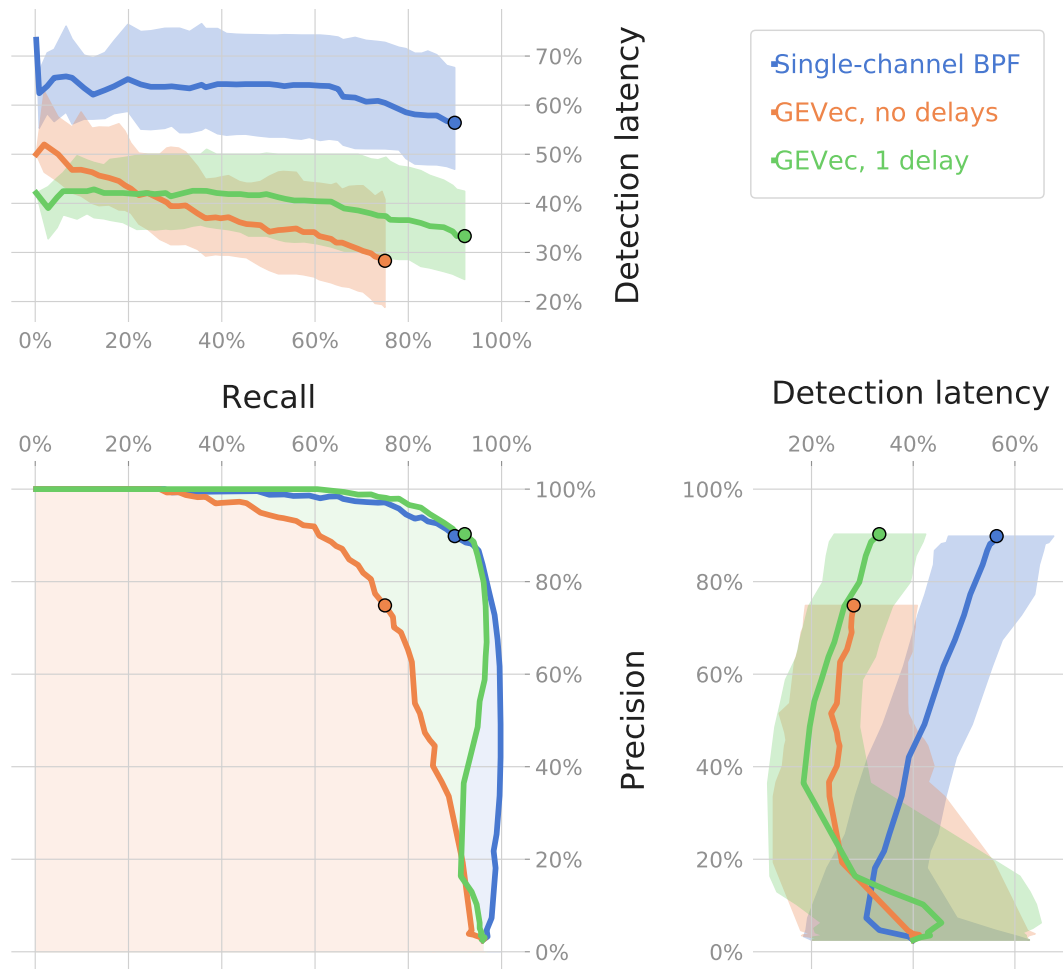
Figure 3.3: **Sensitivity, precision & latency tradeoffs,** for different linear filters & for a range of thresholds.

Each threshold setting for an algorithm corresponds to a point on the precision-recall curve in the bottom-left panel, and to a distribution of relative detection latencies. The median and interquartile range of this distribution are plotted in the top or right panel (as a point of the bold curve or a slice of the shaded band, respectively).

These latency distribution plots are divided over two panels so that their entire range can be clearly visualised, both for the low recall – high precision regime as for high recall – low precision regime. The cutoff is made at the point where recall equals precision (AKA the $\max F_1$ point), marked with shaded black circles.

as was already observed qualitatively. At the aforementioned sensitivity of 80%, the state-of-the-art method has a precision of 94%, whereas the GEVec-based method has a precision of only 63% (i.e. more than a third of detected events are classfied as 'false positives'). This strong decrease in precision is true over the entire PR-curve: see fig. 3.3.

3.6   Combining space and time [1p]

It is hardly surprising that the GEVec-based algorithm as described above cannot discern ripple activity (which is by definition a temporal pattern), as the algorithm is a purely *spatial* filter: at each timestep t, only current information from the different channels is used in calculating the output o_t, without incorporating temporal information from previous timesteps $t_p < t$.

The GEVec method can be easily adapted to also incorporate temporal information however, by defining a vector $\mathbf{z}_t^{\text{stack}} \in \mathbb{R}^{CP}$ which consists of stacked sample vectors (each consisting of C channels) from P different timesteps $t_p \leq t$. The linear weights $\mathbf{w}^{\text{stack}} \in \mathbb{R}^{CP}$ used to obtain the output signal $o_t = (\mathbf{w}_t^{\text{stack}})^T \mathbf{z}_t^{\text{stack}}$ are then calculated analogously to the purely spatial filter, i.e. as the first generalised eigenvector of the ordered pair $(\mathbf{R}_{SS}^{\text{stack}}, \mathbf{R}_{NN}^{\text{stack}})$, with both covariance matrices $\in \mathbb{R}^{CP \times CP}$.

Adding just one such delayed timestep (i.e. $P = 2$) yields a major performance improvement (fig. 3.3): ...

The GEVec and an example of its output envelope is shown in fig. 3.2 (green envelope).

3.7   Regularization [1p]

3.8   Channels [1p]

3.9   Delays [1p]

3.10   Multiple eigenvectors [2p]

3.11   Spectral preprocessing [1p]

Chapter 4

Nonlinear signal detection − 2 Nov [9p]

4.1 Recurrent neural networks [2p]

4.2 Optimization [3p]

4.3 Regularization [2p]

4.4 Channels [1p]

4.5 Network size [1p]

Chapter 5

Discussion – 16 Nov [4p]

5.1 Comparing detectors [2p]

5.2 Further work [2p]

Conclusions – 30 Nov [1p]

References

[1] C. J. Van Rijsbergen. *Information Retrieval*. 2nd. Newton, MA, USA: Butterworth-Heinemann, 1979. ISBN: 0-408-70929-4. URL: `http://www.dcs.gla.ac.uk/Keith/Preface.html`.

[2] Gene H. Golub and Charles F. Van Loan. *Matrix Computations*. Fourth edition. The Johns Hopkins University Press, 2013.

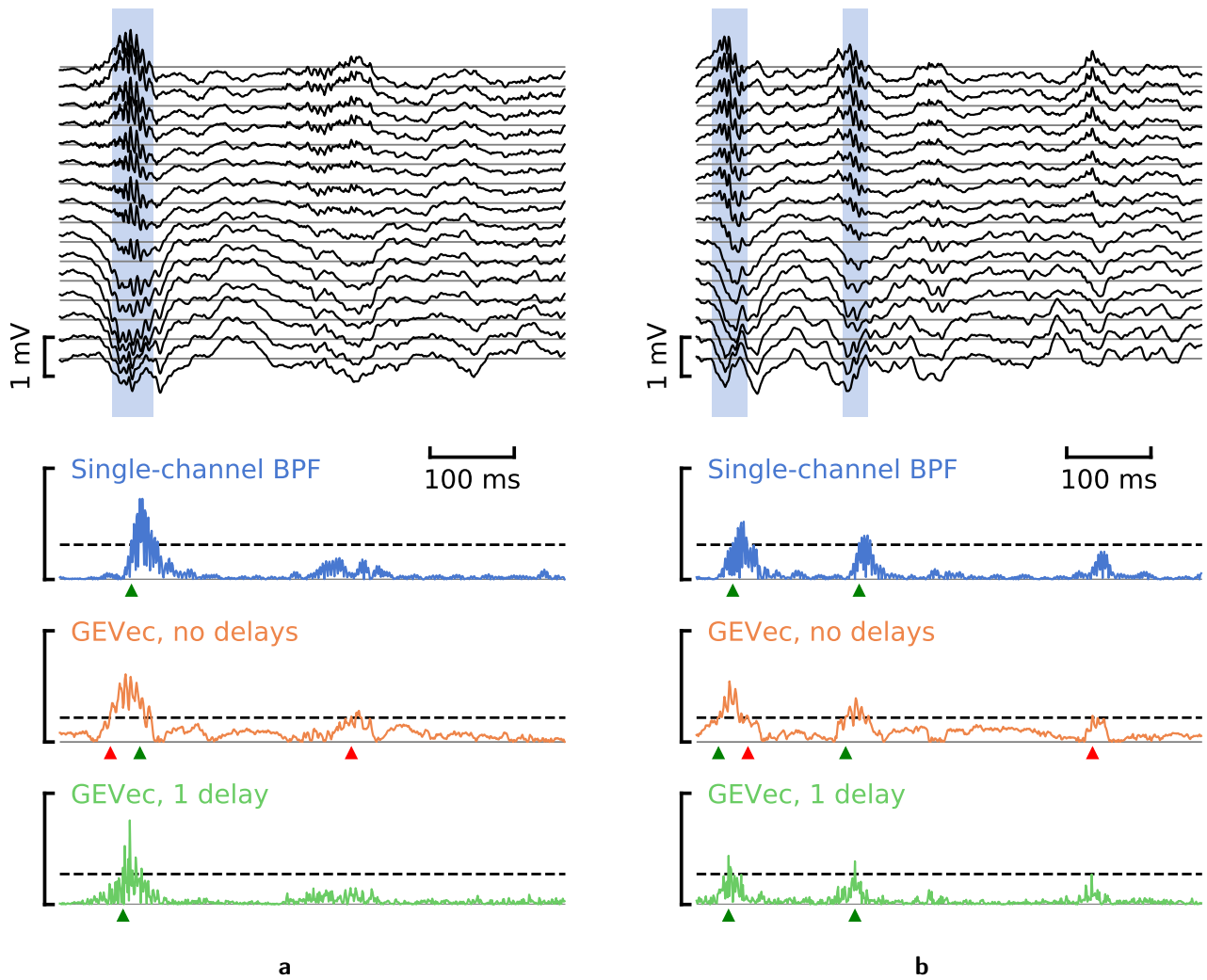# Appendices

Appendix A

Data description

Appendix B

Generalized eigenvectors maximise signal-to-noise

Appendix C
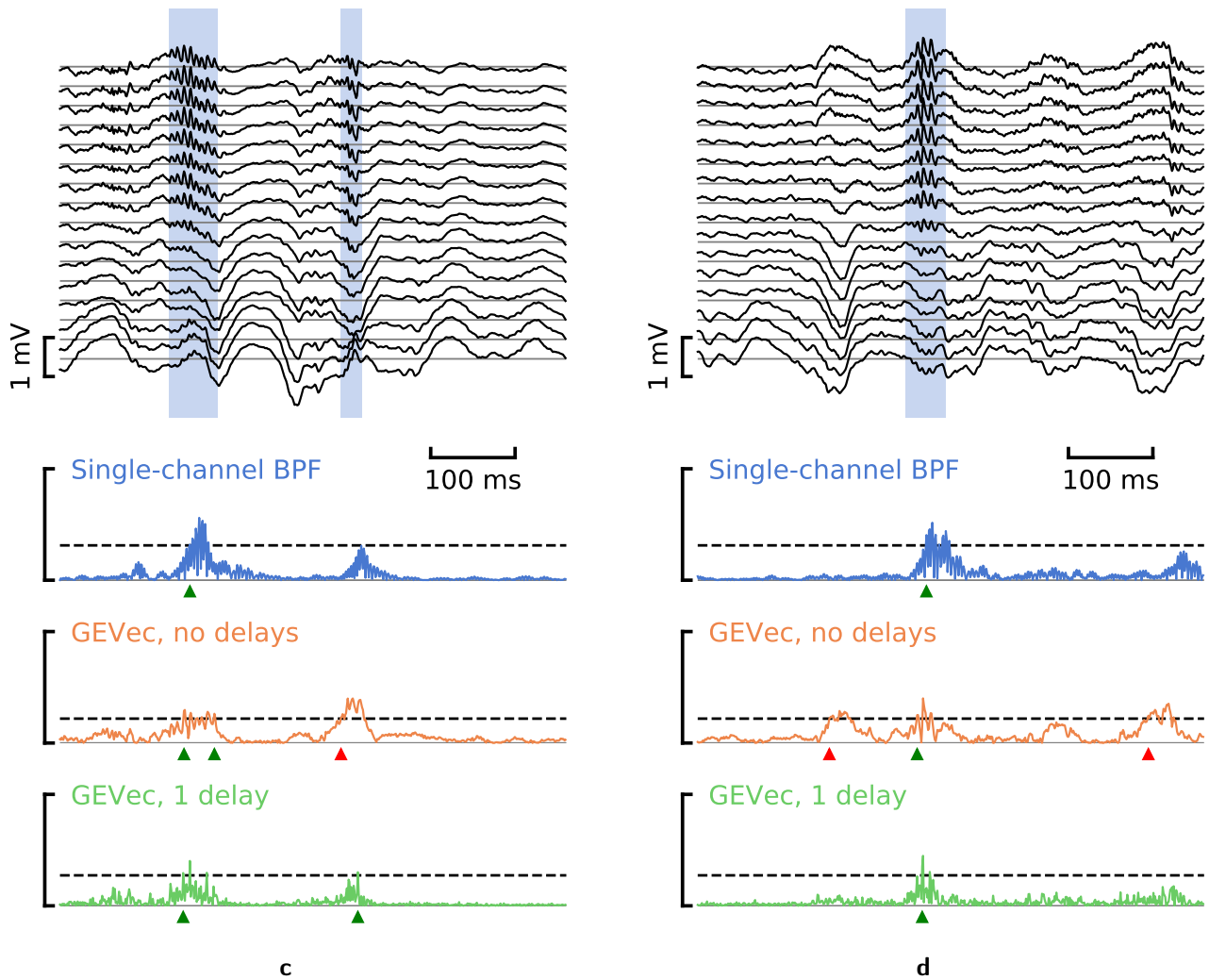
Supplemental figures

Figure C.1: **Extracts from input data and corresponding linear filter output envelopes**. See fig. 3.2 for legend.